RAA 2014 Vol. **14** No. **8**, 992–1000 doi: 10.1088/1674–4527/14/8/009
http://www.raa-journal.org *http://www.iop.org/journals/raa*

Research in Astronomy and Astrophysics

Improved astrometry of space debris with image restoration *

Rong-Yu Sun and Chang-Yin Zhao

Purple Mountain Observatory, Chinese Academy of Sciences, Nanjing 210008, China; *cyzhao@pmo.ac.cn*
Key Laboratory of Space Object and Debris Observation, Chinese Academy of Sciences, Nanjing 210008, China

Received 2013 December 1; accepted 2014 February 18

Abstract In order to implement an observing strategy, image degradation that occurs during optical observation of space debris is ineluctable and has distinct characteristics. Image restoration is presented as a way to remove the influence of degradation in CCD images of space debris, based on assumed PSF models with the same FWHM as images of the object. In the process of image restoration, the maximum entropy method is adopted. The results of reduction using observed raw CCD images indicate that the precision in estimating positions of objects is improved and the effects of degradation are reduced. Improving the astrometry of space debris using image restoration is effective and feasible.

Key words: techniques: image processing — space vehicles — astrometry — methods: data analysis

1 INTRODUCTION

Image restoration is defined as the reconstruction of an image by means of the removal of degradation (Beauchamp & Yuen 1979). During the image reconstruction process, the degradation is removed by spatial filtering or frequency deconvolution. Image restoration is a key area in signal and image processing, which can be used for deblurring, removal of atmospheric seeing degradation and tracking errors, etc (Starck & Pantin 2002). Restoration of astronomical images has been demonstrated in some cases to be crucial for specific objectives; for instance, image reconstruction that was applied to the Hubble Space Telescope before the detector system was refurbished (White 1994). This technique should be used in more applications to take advantage of ground-based optical telescopes, whose image quality is strongly affected by degradation.

Space debris poses an increasing threat for current and future space operations (Schildknecht 2007). To avoid the risks caused by space debris in space missions (Xu & Xiong 2013, 2014), information about these objects must be continuously collected and maintained. In order to implement the current observing strategy (Sun & Zhao 2013), image degradation in optical observation of space debris can be a tool to overcome serious challenges present in this process. In particular, there is relative movement between the observed object and background stars (Sun & Zhao 2012a), and the images of the object appear as points while the images of the stars show up as streaks. Considering that if the images of background stars are elongated too much, this will affect the centroid estimation.

* Supported by the National Natural Science Foundation of China.

In addition, the effective integration time of exposure is limited, which may make the surface distribution of images taken of objects irregular. Meanwhile, due to the generally large angular velocity of space debris, the telescope should move with the same angular velocity to make images of the object appear at the center of the field of view, so tracking errors of the telescope during fast movement are significant (Tang et al. 2001). Furthermore, a large field of view is required for telescopes dedicated to surveying space debris, which may sometimes lead to undersampling (Lauer 1999). Image degradation affects the quality of observed CCD images and causes additional errors in centroid estimations, which should be resolved to acquire precise astrometry of space debris.

Recently, several image processing algorithms with spatial filtering have been demonstrated to be effective in improving the precision in measuring space debris (Sun & Zhao 2013). In this paper, image restoration techniques, based on frequency deconvolution, are introduced to remove the influence of image degradation in optical observation of space debris. In application, the maximum entropy method (Bontekoe et al. 1994; Pantin & Starck 1996) is adopted, and we expect to improve the precision in measuring the location of space debris with this method. The basic theories of image degradation and the maximum entropy method are introduced in Section 2. Application of the maximum entropy method in data reduction is presented in Section 3 and the results as well as discussions are shown in Section 4. Section 5 gives the conclusion.

2 BASIC THEORIES AND PRINCIPLES

For a spatially linear and shift-invariant system, $I(x, y)$ is a two-dimensional output image, which can be considered to be the image we observed that was blurred by image degradation. $I(x, y)$ corresponds to the observation of an initial image characterized by the intensity distribution $O(x, y)$. The relation between the observed data and the initial ones at the same coordinate can be expressed as (Starck & Murtagh 2006)

$$I(x, y) = O(x, y) \otimes H(x, y) + N(x, y)\,, \tag{1}$$

where $N(x, y)$ is the additive noise of the system, (x, y) represents the spatial coordinates of the images, and $\otimes$ denotes convolution. In general, $H(x, y)$ represents the Point Spread Function (PSF) of the imaging system (Popowicz et al. 2013), which is defined as the output of the system while the input signal is a point source of light. The PSF can usually be modeled by a Gaussian surface for a high quality telescope system if the exposure time is long enough. However, in application the component $H(x, y)$ is much more complicated and it may be affected by other factors (e.g. the spatial form of the pixel), hence the form of $H(x, y)$ should be determined carefully.

Accordingly, in Fourier space, we have (Starck & Murtagh 2006)

$$\hat{I}(u, v) = \hat{O}(u, v) \times \hat{H}(u, v) + \hat{N}(u, v)\,, \tag{2}$$

where $\hat{H}(u, v)$ is the transform of $H(u, v)$, while $\hat{I}(u, v)$, $\hat{O}(u, v)$ and $\hat{N}(u, v)$ are the transforms of the blurred image, the initial image and the noise, respectively.

Image restoration determines the true image $O(x, y)$ with a priori information about the blurring model $H(x, y)$ and the noise model $N(x, y)$. Obviously, a simple division can be done between $\hat{I}$ and $\hat{H}$

$$\hat{O}(u, v) = \frac{\hat{I}(u, v)}{\hat{H}(u, v)} - \frac{\hat{N}(u, v)}{\hat{H}(u, v)}\,. \tag{3}$$

Then, the estimated image $O(x, y)$ can be obtained by computing the Fourier transform of the deconvolved one $\hat{O}(u, v)$. However, due to the cut-off frequency of $\hat{H}(u, v)$ and the presence of additive noise, this method cannot be used.

Generally in practice, Equation (1) is an ill-posed problem, which means there is no unique, stable solution. Various algorithms have been developed to recover a best estimation of the true

image $O(x, y)$; for example, Wiener filtering (Press et al. 1986), the Richardson-Lucy algorithm (Lucy 1974) and iterative blind deconvolution (Jefferies & Christou 1993).

Considering that the noise level is significant for observation of space debris, and that the noise may be highly variable with time, it is difficult to define a noise model. Meanwhile, due to the unavoidable noise and spurious instrument signatures, the image degradation that occurs in surveys of space debris is inevitable and has special characteristics, which makes it difficult to construct the PSF from the data. Hence, during image restoration, the maximum entropy method (Starck & Murtagh 2001) is adopted, which needs no a priori model for the noise and can be generalized to many different noise distributions, and approximated PSF models are chosen in implementation.

Let $p(O)$ denote the probability of the true image over all possible image realizations. The maximum entropy method derives this probability of O from its entropy, and we obtain the solution by maximizing $p(O)$. The maximum entropy method makes the assumption that the solution O is positive, and it does not need any other a priori information. In application, we chose the entropy function defined by Frieden (1979)

$$M_f(O) = -\sum_x \sum_y O(x, y) \ln O(x, y) \,, \tag{4}$$

where the probability of the true image can be derived as

$$p(O) = \exp[-\alpha M(O)] \,, \tag{5}$$

and the solution is estimated iteratively during processing (Liu et al 2010).

3 APPLICATIONS

Raw CCD images are made to investigate the efficiency of image restoration. The raw CCD images are acquired from a 50-cm optical telescope dedicated to surveying space debris. The corresponding parameters of this telescope are listed in Table 1. During observations, two GPS satellites are observed. Considering that the CCD images of GPS satellites are similar to those of space debris, and the precise ephemerides for GPS satellites are provided with a precision better than 1 m, which can be taken as the reference position at observing times, it is reliable and effective to test image restoration using images of these satellites. The results for GPS satellites agree with those for space debris.

Table 1 Parameters Describing the Telescope

Parameter	Value
Image size	2048×2048
Field of view	$4.4^\circ \times 4.4^\circ$
Spatial sampling	$7.73''$
CCD operating mode	Full frame
Number of channels	4

It should be noted that the field of view of the telescope is relatively large, which leads to poor spatial sampling, hence the measurement accuracy of objects is affected.

A sample raw CCD image is shown in Figure 1. Considering that the field of view of our telescope is large, as in many wide field systems, the vignetting is obvious. For the full frame CCD camera, the smear noise is ineluctable without the use of a shutter (Sun et al. 2012b), which affects the quality of our image. Furthermore, the CCD image is read out through four channels. Each channel has a different readout noise, hence the background of the whole image is composed of four levels. It is obvious that the image can be divided into four blocks based upon the background

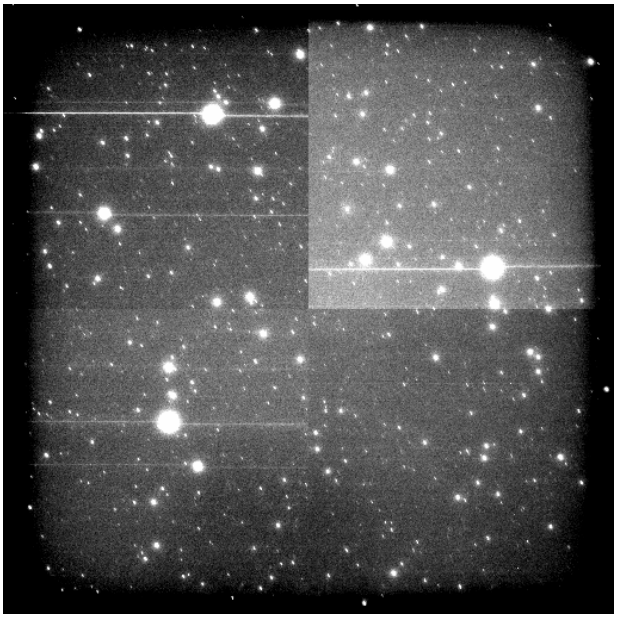

Fig. 1 A sample of a raw CCD image acquired during observations.

level. Due to the observing strategy adopted, the images of objects usually appear at the center of the frame; variable background levels may cause additional errors in astrometry.

After the observations, 12 arcs from raw CCD images are obtained. As mentioned above, in image restoration, the PSF should be assumed to be known. In practice, the PSF is usually constructed from the data or the optical model of the imaging system. However, for observation of space debris, due to degradation (e.g. limited effective integration time, elongated star images, significant tracking errors, etc), the PSF is highly variable with time and it is difficult to implement these approaches. Here we present a simple approximate method to give the PSF. In detail, we measure the full width at half maximum (FWHM) for images of objects, and choose PSF models with a similar FWHM as one of these images. A listing of the FWHM of the object is shown in Table 2. It is easily found that the FWHM of objects is around 2.5 pixels. The large size of the PSF matrix leads to a significant cost in computing time. In applications, two PSF models with FWHM$=2$ pixels are adopted, and the size of the PSF matrix is limited to 3×3. The FWHM of the two PSF models we give is slightly less than the one acquired from images of objects. The first is the Gaussian model (PSF1), while the other is the widely used SExtractor (Bertin & Arnouts 1996). The two models are listed as follows.

$$\mathrm{PSF1}=\begin{pmatrix} 0.260856 & 0.483068 & 0.260856 \\ 0.483068 & 0.894573 & 0.483068 \\ 0.260856 & 0.483068 & 0.260856 \end{pmatrix}, \tag{6}$$

$$\mathrm{PSF2}=\begin{pmatrix} 1 & 2 & 1 \\ 2 & 4 & 2 \\ 1 & 2 & 1 \end{pmatrix}. \tag{7}$$

Using the two models above, image restoration is applied to all of the raw CCD images. The SExtractor software is then applied to both the original images and deconvolved images, extracting the source information; for example, the pixel coordinates of the center of the star and center of the object. With these pixel positions, the astronomical calibration is implemented and the observed

Table 2 Information about the Arcs

Arc ID	Number of frames	Average number of background stars	Listing of object FWHM (pixel)
1	52	290.59	2.60±0.13
2	57	362.68	2.65±0.34
3	40	293.79	2.62±0.73
4	54	368.25	2.57±0.06
5	54	369.27	2.65±0.12
6	50	373.21	2.65±0.13
7	54	362.57	2.67±0.11
8	29	364.08	2.59±0.06
9	80	305.84	2.66±0.34
10	53	303.61	2.65±0.22
11	55	371.00	2.55±0.07
12	53	362.94	2.87±0.91

equatorial coordinates of the satellites $(\alpha_{\rm o}, \delta_{\rm o})$ are obtained. During astronomical calibration, stars brighter than magnitude 12 in the Tycho2 catalog (Hog et al. 2000) are used; considering that the field of view of the telescope is large, this number of background stars is sufficient. Finally, the equatorial coordinates obtained by astronomical calibration are compared with the reference coordinates $(\alpha_{\rm c}, \delta_{\rm c})$, which are interpolated from the precise ephemeris. The resultant deviations $(\sigma_\alpha, \sigma_\delta)$ are computed as

$$\begin{cases} \sigma_\alpha = (\alpha_{\rm o} - \alpha_{\rm c}) \times \cos\delta_{\rm c}\,, \\ \sigma_\delta = \delta_{\rm o} - \delta_{\rm c}\,. \end{cases} \tag{8}$$

We regard the Root Mean Square (RMS) values of all the deviations in the same arc as the precision of reduction. The related details of all of the 12 arcs (e.g. number of frames) and the average number of stars during astronomical calibration are listed in Table 2.

4 RESULTS AND DISCUSSION

Figure 2 shows the whole process of reduction, in which six sets of sample images of objects are listed as an example. The left column shows the contour plots of the six object images before the restoration process is applied, the middle column shows the contour plots of the resultant object images deconcolved with PSF1, and the right column presents those with PSF2. The measured errors of these six objects are shown in Table 3, including the error in Right ascension (RA) and the error in Declination (Dec).

From the panels in Figure 2, it can be easily found that before image restoration the intensity distributions of object images are slightly more smooth and spread out, and after restoration, the object images become sharper. As shown in Table 3, image restoration is an effective tool to remove the negative influence of image degradation and improve the precision of astrometry. Most initial

Table 3 Measured Errors in the Six Sample Images

Image ID	Initial errors ($''$)		Errors with PSF1 ($''$)		Errors with PSF2 ($''$)	
	RA	Dec	RA	Dec	RA	Dec
1	–3.46	–2.85	–1.98	0.01	–1.83	0.73
2	–1.81	1.08	–0.83	0.17	–0.85	0.27
3	–1.42	–2.33	–1.42	–0.62	–1.39	–0.56
4	–1.31	0.58	–0.40	0.67	–0.41	0.63
5	–1.07	–1.70	–0.59	–1.03	–0.36	–0.83
6	1.20	–1.12	0.07	–0.89	–0.18	–0.91

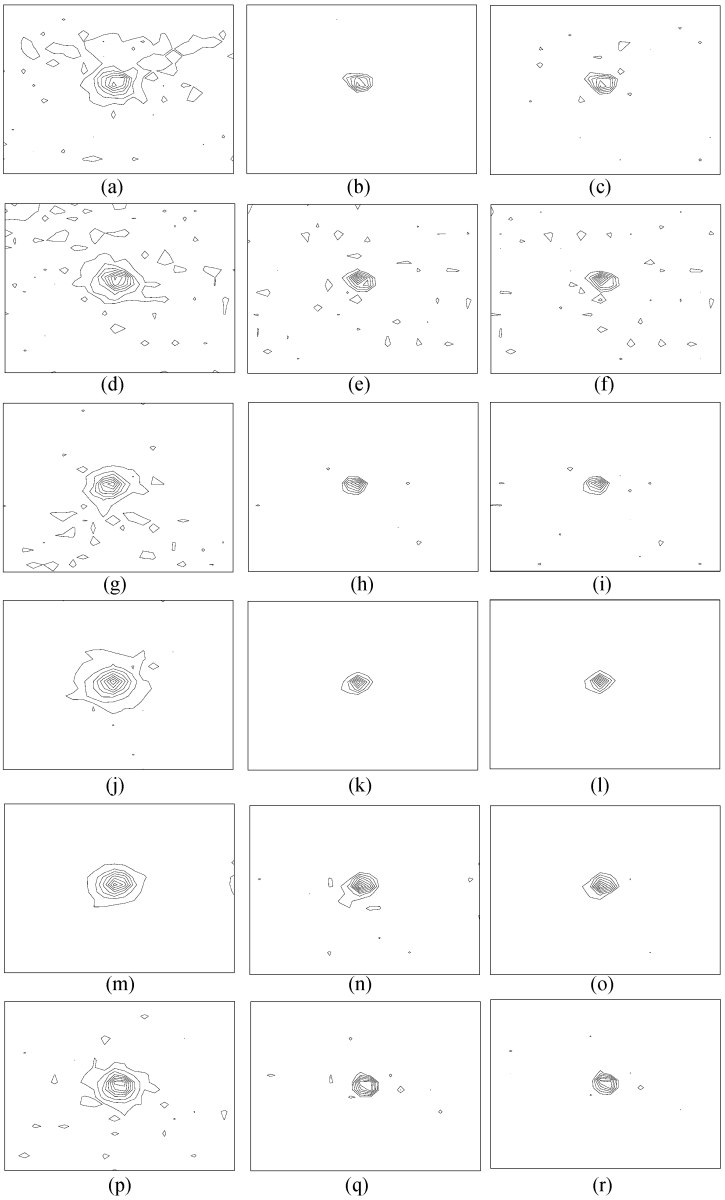

Fig. 2 Contour plots of the six sample images. (a), (d), (g), (j), (m) and (p): initial image; (b), (e), (h), (k), (n) and (q): deconvolved with PSF1; (c), (f), (i), (l), (o) and (r): deconvolved with PSF2.

measurement errors in these six images are around $1.5''$, and considering that the pixel scale is $7.73''$, this precision is relatively good. After restoration, the measurement errors of these six sample images are significantly reduced, and the improvement is clearly evident. Which of the two PSF models that are used does not make much difference in improving the astrometry.

The results of the applications on all the 12 arcs are shown in Table 4. The effect and efficiency of the two PSF models are similar, because both improve the measurement precision of object images. For the 12 arcs, the increase in accuracy of 10 arcs is greater than 10%, and three arcs have

Table 4 Improvement in Precision for All Arcs

Arc ID	Initial RMS of deviations /arc	RMS of deviations after restoration /arc		Increase (%)	
		PSF1	PSF2	PSF1	PSF2
1	1.79	1.30	1.21	27.10	32.46
2	1.23	1.14	1.13	7.08	7.94
3	1.92	1.29	1.33	32.94	30.75
4	1.58	1.28	1.26	19.20	19.95
5	1.41	1.18	1.22	15.88	13.18
6	1.33	1.18	1.23	11.05	7.81
7	1.27	1.06	1.12	16.52	11.88
8	1.50	0.97	1.07	34.96	28.52
9	1.61	1.50	1.47	6.49	8.31
10	1.33	1.19	1.23	10.74	7.67
11	1.81	1.42	1.35	21.70	25.42
12	1.53	0.99	1.02	34.95	33.29

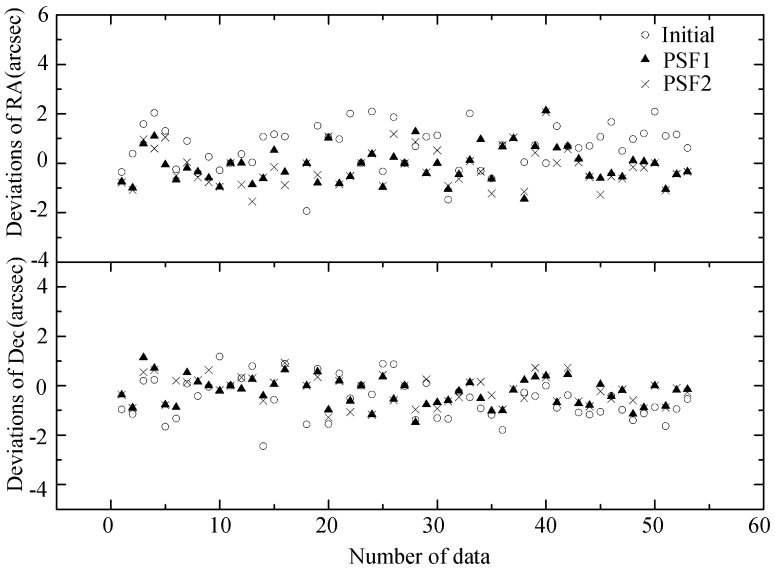

Fig. 3 Deviations of object positions in arc 3. *Circles*: initial images. *Triangles*: deconvolved with PSF1. *Crosses*: Deconvolved with PSF2.

increases greater than 30%. It is evident that using image restoration reduces the influence of degradation and improves the astrometry for space debris. It is also demonstrated that the assumptions and approximations we made when deciding the PSF model are reliable. Although the PSF model is not constructed from the experimental data or the optical model of the imaging system, in practice we assume the PSF model has a similar FWHM to the object images and gives two simple models. The result shows that this works effectively. For any other arbitrary PSF models, the astrometry seems to be improved as long as the model is similar to the real one. Obviously, the best image restoration will be derived if an accurate imaging degradation model is provided. However, an accurate PSF model is hard to acquire, and making some suitable approximations during processing returns reliable results.

The values of deviation for both RA coordinates and Dec coordinates for arc 3 and arc 12 are taken as an example, and they are shown in Figures 3 and 4 respectively. The values of deviations for

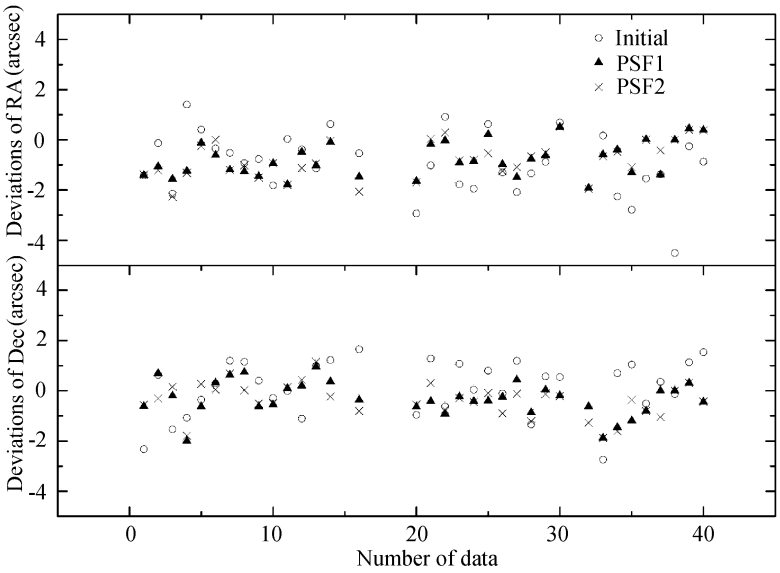

Fig. 4 Deviations of object positions in arc 12. *Circles*: initial images. *Triangles*: deconvolved with PSF1. *Crosses*: Deconvolved with PSF2.

all the three types of data are around $0''$, from about $-2''$ to $2''$, which indicates that the systematic errors in our system are not prominent and that the random errors in measurement play the dominate role. Image restoration reduces the random errors, leading to a smaller range of values for deviations. The improvement by image restoration is consistent for all the data in the whole arc, and the effect of a variable PSF model makes no difference.

5 CONCLUSIONS

Due to the observing strategy and instrumental effects, the imaging degradation for CCD images of space debris have special properties. Degradation affects the imaging quality of the system and increases errors associated with measuring the object. An image restoration approach is adopted to remove the negative influences of image degradation and improve the astrometric precision of objects. In practice, the maximum entropy method is chosen, considering that little a priori information about the degradation process can be used. During application, it is difficult to construct the PSF from experimental data or the optical system; hence, we make an approximation and provide two PSF models with similar FHWM values as the object images. In total, 12 arcs appear on raw CCD images taken of GPS satellites that are acquired to test the efficiency of image restoration. The results indicate that image restoration removes the influence of imaging degradation and improves the precision in measuring the positions of satellites. The increase in accuracy can be more than 30%, and variable PSF models do not make much difference in data reduction. The GPS satellites have similar characteristics as space debris in terms of observation; hence, the application of image restoration can be extended to the data reduction of space debris, and the efficiency is analogous.

Acknowledgements This work was funded by the National Natural Science Foundation of China (Grant Nos. 11125315 and 11033009).

References

Beauchamp, K. G., & Yuen, C. K. 1979, Digital Methods for Signal Analysis (New York, NY: Routledge)
Bertin, E., & Arnouts, S. 1996, A&AS, 117, 393
Bontekoe, T. R., Koper, E., & Kester, D. J. M. 1994, A&A, 284, 1037
Frieden, B. R. 1979, Image Enhancement and Restoration, in Picture Processing and Digital Filtering, Topics in Applied Physics, 6, 177 (Berlin: Springer)
Høg, E., Fabricius, C., Makarov, V. V., et al. 2000, A&A, 355, L27
Jefferies, S. M., & Christou, J. C. 1993, ApJ, 415, 862
Lauer, T. R. 1999, PASP, 111, 227
Liu, H. B., Shen, J., Guo, S., et al. 2010, Digital Image Processing Using Visual C++ (Beijing: China Machine Press)
Lucy, L. B. 1974, AJ, 79, 745
Pantin, E., & Starck, J.-L. 1996, A&AS, 118, 575
Popowicz, A., Kurek, A. R., & Filus, Z. 2013, PASP, 125, 1119
Press, W. H., Flannery, B. P., & Teukolsky, S. A. 1986, Numerical Recipes. The Art of Scientific Computing (Cambridge: Cambridge Univ. Press)
Schildknecht, T. 2007, A&A Rev., 14, 41
Starck, J. L., & Murtagh, F. 2006, Astronomical Image and Data Analysis (Berlin: Springer)
Starck, J.-L., Murtagh, F., Querre, P., & Bonnarel, F. 2001, A&A, 368, 730
Starck, J. L., Pantin, E., & Murtagh, F. 2002, PASP, 114, 1051
Sun, R., Zhao, C., & Zhang, Y. 2012a, Science in China: Physics, Mechanics and Astronomy, 55, 1945
Sun, R.-Y., Zhao, C.-Y., Ping, Y.-D., Xiong, J.-N., & Zhang, C. 2012b, Chinese Astron. Astrophy., 36, 340
Sun, R.-Y., & Zhao, C.-Y. 2013, RAA (Research in Astronomy and Astrophysics), 13, 604
Sun, R.-Y., Zhao, C.-Y., & Zhang, Y.-P. 2013, PASJ, 65, 110
Tang, Z.-H., Wang, S.-H., & Jin, W.-J. 2001, AJ, 121, 1199
White, R. L. 1994, in Astronomical Society of the Pacific Conference Series, 61, Astronomical Data Analysis Software and Systems III, eds. D. R. Crabtree, R. J. Hanisch, & J. Barnes, 292
Xu, X.-L., & Xiong, Y.-Q. 2013, Science in China: Physics, Mechanics and Astronomy, 56, 1041
Xu, X., & Xiong, Y. 2014, RAA (Research in Astronomy and Astrophysics), 14, 601